

# Accretion disc MHD winds and blazar classification

Stella Boula,<sup>1</sup>★ Demosthenes Kazanas<sup>2</sup> and Apostolos Mastichiadis<sup>1</sup>

<sup>1</sup>Department of Physics, National and Kapodistrian University of Athens, Panepistimiopolis, GR 15783 Zografos, Greece

<sup>2</sup>NASA Goddard Space Flight Center, Greenbelt, MD 20771, USA

Accepted 2018 October 3. Received 2018 October 3; in original form 2018 July 23

## ABSTRACT

The Fermi Gamma-Ray Space Telescope observations of blazars show a strong correlation between the spectral index of their  $\gamma$ -ray spectra and their synchrotron peak frequency  $\nu_{\text{pk}}^{\text{syn}}$ ; additionally, the rate of Compton dominance of these sources also seems to be a function of  $\nu_{\text{pk}}^{\text{syn}}$ . In this work, we adopt the assumption that the non-thermal emission of blazars is primarily due to radiation by a population of Fermi-accelerated electrons in a relativistic outflow (jet) along the symmetry axis of the blazar’s accretion disc. Furthermore, we assume that the Compton component is related to an external photon field of photons, which are scattered from particles of the magnetohydrodynamic wind emanating from the accretion disc. Our results reproduce well the aforementioned basic observational trends of blazar classification by varying just one parameter, namely the mass accretion rate on to the central black hole.

**Key words:** Acceleration of particles – radiation mechanisms: non-thermal – galaxies: active.

## 1 INTRODUCTION

Blazars (Flat Spectrum Radio Quasars and BL Lacs) are types of active galactic nuclei (AGNs) with relativistic jets pointing towards us. The relativistic motion of these jets amplifies their radiation emission, which in general dominates their disc emission, making these objects extremely bright and therefore visible at large redshifts,  $z$ . The blazar jet spectra are non-thermal *par excellence*, implying emission by inherently relativistic electron distributions. They consist of two broad ‘humps’, one that spans the radio to optical-UV (and occasionally the X-ray) bands and another one that extends from X-rays to multi-GeV and on occasion to TeV  $\gamma$ -rays. The first is thought to be due to synchrotron emission by the jet’s non-thermal electrons and peaks in the IR–X-ray band, while the second by inverse Compton (IC) scattering of the synchrotron or external (from an altogether different source) photons. Quasi-simultaneous multi-wavelength variability is also observed but not always, suggesting that the broader emission of both ‘humps’ spans a region larger than that over which the electrons, radiating at a specific band, cool. The size of the emitting region is also not well established; the typical size estimates obtained from temporal variability arguments are affected by relativistic plasma motion and radiative cooling. It varies among sources and even among different observations of the same object and depends on the processes employed to model the emission in specific bands. A typical emission region, at least in FS-RQs where line emission is detected, is thought to be the broad line region (Sbarrato et al. 2012), of the order of  $R_{\text{BLR}} \sim 10^3 - 10^4 r_{\text{Sg}}$  [where  $r_{\text{Sg}} \simeq 3 \times 10^{13} (M/10^8 M_{\odot})$  cm is the Schwarzschild radius

of the black hole of mass  $M$ ]. On the other hand, the apparently thin GeV emission (Marscher et al. 2010) suggests a location (at least of this emission) at a distance as large as  $\sim 10^6 r_{\text{Sg}} \sim 10$  pc, considerably larger than  $R_{\text{BLR}}$ .

One would think that the broad frequency range of blazar emission, their multiscale variability and the strong dependence of the observed luminosity on the bulk Lorentz factor of the relativistic jets and the observers’ line of sight relative to its motion, would preclude a systematic study of the blazar properties. Indeed, fits to their individual multiwavelength spectra in terms of Synchrotron – Compton models require no less than seven parameters (Ghisellini et al. 2011). However, even with the limited  $\gamma$ -ray data of *CGRO*, certain regularities became apparent and are now known as the ‘Blazar Sequence’ (Fossati et al. 1998): Blazars become redder with increasing bolometric luminosity  $L_{\text{bol}}$ , in that their synchrotron peak frequency  $\nu_{\text{pk}}^{\text{syn}}$  decreases as  $L_{\text{bol}}$  increases; at the same time their Compton dominance (CD) (i.e. the ratio of their IC to synchrotron luminosities) increases and so do their  $\gamma$ -ray spectral indices.

The blazar sequence, established with 132 objects out of which only 33 were detected in high-energy  $\gamma$ -rays, was supplanted with the launch of *Fermi* and the discovery of more than 1000  $\gamma$ -ray blazars in the 2nd and 3rd Fermi Blazar Catalogs (2LAC, 3LAC) (Ackermann et al. 2011, 2015), half of which with measured redshifts. These compilations provided novel correlations that replaced those of the original blazar sequence. Most importantly, these correlations were found to be independent of the source luminosity, implying that the underlying physics are related to dimensionless parameters. These correlations relate the slope  $\alpha_{\gamma}$  of the  $\gamma$ -ray spectrum to the synchrotron peak frequency  $\nu_{\text{pk}}^{\text{syn}}$  (Figs 17 and 10 of 2LAC and 3LAC, respectively) and the CD to  $\nu_{\text{pk}}^{\text{syn}}$  (fig. 27 of 3LAC; see also Finke 2013).

\* E-mail: [stboula@phys.uoa.gr](mailto:stboula@phys.uoa.gr)

Various aspects of the blazar sequence have been put forward by a number of investigators: Ghisellini et al. (1998) suggested it was based on the different radiative cooling suffered by electrons in the different classes of sources, assuming the same heating process in all. In this respect, the more luminous FSRQs rely on the (observed) BLR line emitting clouds to isotropize a non-negligible fraction of the accretion disc luminosity, which is then (inverse) Comptonized by the jet’s accelerated electrons and boosted by its relativistic motion to provide their higher luminosities. BL Lacs with weaker line emission are therefore less luminous and exhibit higher individual electron energies. The dependence of the blazar sequence on  $L_{\text{bol}}$  prompted Nieppola et al. (2008) to suggest that it is the result of different observer orientations and therefore different values of the beaming factor  $\delta$ . Pursuing a different point of view, Ghisellini, Maraschi & Tavecchio (2009) and Ghisellini et al. (2011) suggested that at small (normalized) accretion rates, transition of the accretion flow to an ADAF (Narayan & Yi 1995) state would cause removal of the BLR region, absence of the concomitant cooling and reduction of the  $\gamma$ -ray slope to  $\alpha_\gamma < 1$ , thus ‘dividing’ blazars into FSRQs and BL Lacs on the basis of this parameter. More recently, noting that the dependence of the blazar sequence on the (relativistically boosted) blazar bolometric luminosity sounds non-physical, Ghisellini et al. (2017) proposed an altogether different scheme, separating the BL Lac and FSRQ behaviour, with the former following the well-defined blazar sequence and the latter forming their own distinct class.

This work is motivated by observations and models of an altogether different aspect of AGN phenomenology, namely by features that have been termed ‘Warm Absorbers’. These are blue-shifted absorption features in the X-ray spectra, indicating the presence of ionized outflows, a ubiquitous feature both in the UV and X-ray AGN spectra (Crenshaw, Kraemer & George 2003).

The presence of absorption features is very important for the determination of the properties of these outflows since each such transition ‘lives’ at a well-defined value of the photoionization parameter  $\xi$  ( $= Ln(r)r^2$ , where  $L$  is the ionizing luminosity,  $n(r)$  the plasma density, and  $r$  its distance from the black hole). The entire wind density profile of a transition can be determined by measuring both  $\xi$  and the absorption depth of said transition, along the line of sight. This was the approach of Behar (2009), who, assuming a density profile of the form  $n(r) \propto r^{-p}$ , fitted the multiple absorber data to obtain values of  $p$  close to 1 ( $1 < p \lesssim 1.22$ ). It is important to note that these density profiles are much shallower than those expected in radiation driven winds. Such profiles are naturally produced in self-similar accretion disc magnetohydrodynamic (MHD) winds (Contopoulos & Lovelace 1994; Fukumura et al. 2010), launched over the entire disc domain, spanning a radial range of  $R_D \sim 10^5 - 10^6 r_{\text{sg}}$ . At the same time the winds have a very steep density dependence on the polar angle  $\theta$ . The steep  $\theta$  dependence gives to these winds a toroidal appearance, considered for this reason to be the ‘dusty tori’ invoked in AGN unification (Antonucci & Miller 1985; Konigl & Kartje 1994). The shallow radial density profile of these winds is of importance in the determination of the blazar radiative properties: it allows the scattering of the accretion disc’s continuum radiation over large distances, so that it becomes roughly isotropic over radii comparable to the extent of the disc ( $r \sim R_D$ ). This radiation will then appear in the forward direction on the frame of the relativistic jet out to distances  $r_z$  along its axis, such that  $r_z/\Gamma \sim R_D$  ( $\Gamma$  is the bulk Lorentz factor). It can then be scattered efficiently by the high-energy electrons of the relativistically moving jet to produce its observed X-ray and  $\gamma$ -ray radiation; these are the photons employed in the external Compton (EC) scat-

tering that appear to produce the dominant component of the *Fermi* blazar spectra. The density of these photons is related to the mass accretion rate  $\dot{m}$ , normalized to the Eddington rate. Assuming the magnetic field to be in equipartition with the kinetic energy density, it can be shown that the magnetic energy density is a factor of  $\dot{m}$  (or  $\dot{m}^2$  in the ADAF case) larger than that of the continuum luminosity isotropized through scattering in the wind. However, the latter will be larger than the former by a factor of  $\Gamma^2$  on the jet frame. Therefore, it is expected that the IC will be larger than the synchrotron component when  $\dot{m}\Gamma^2 > 1$ , providing a vestige of the blazar LAT correlations in terms of a single parameter, namely  $\dot{m}$ .

This work provides a detailed study of this argument. In Section 2 we outline the model in more detail, with particular emphasis on the wind structure, the radiation and magnetic fields and the shape of electron distribution function. In Section 3 we compare the results of our models with the LAT blazar correlations, and we summarize and discuss our results in Section 4.

## 2 MODELLING THE BLAZAR SEQUENCE

Previous studies (Fossati et al. 1998) have shown the existence of a Blazar classification, known as Blazar Sequence, which presents a connection between the observed bolometric luminosity and the spectral energy distribution (SED) of blazars. In general, the blazar SED is modelled with a simple one-zone leptonic model (Finke 2013). In this case, accelerated electrons produce a low-energy component through synchrotron radiation and a high-energy one through IC scattering. For the latter component, the origin of the target photon field can be either internal (from synchrotron radiation) and/or external (Dermer, Schlickeiser & Mastichiadis 1992; Sikora, Begelman & Rees 1994).

In this paper, we will also employ this one-zone leptonic model; however, before doing so, we will present simple scalings of all the important parameters on just two fundamental physical quantities of the problem, namely the mass of the black hole and the mass accretion rate.

### 2.1 Scaling of the physical parameters

We begin by calculating the specifics of the external photon field. This is based on the self-similar MHD accretion disc wind model of Fukumura et al. (2010) and the wind is described by steady-state, non-relativistic equations, which include gravity and pressure. These authors derive a density profile for the wind particles of the form

$$n(r, \theta) = n_0(r_s/r)^p e^{5(\theta-\pi/2)}, \quad (1)$$

where  $n_0 = \frac{\eta_w \dot{m}}{2\sigma_T r_s}$ ,  $r_s$  is the Schwarzschild radius,  $\sigma_T$  is the Thomson cross-section,  $\dot{m}$  is the normalized mass accretion rate ratio to the Eddington one, and  $\eta_w$  is the ratio of the mass outflow rate of the wind to the mass accretion rate  $\dot{m}$ , which is assumed to be  $\eta_w \simeq 1$ . The value of the index  $p$  is between 1 and 1.2 (Fukumura et al. 2017, 2018); here, for simplicity we will assume  $p = 1$ , while different values will be explored in a future publication.

As a first-order approximation, we can ignore the dependence of  $n(r, \theta)$  on the polar angle  $\theta$ . In that way one is able to calculate analytically the optical depth of the wind particles to disc photons scattering. Setting therefore at equation (1)  $p = 1$  and assuming a region between any radii  $R_1$  and  $R_2$  (as they are measured from the

central object), the Thomson optical depth can be written as

$$\tau_{\tau}(R_1, R_2) = \int_{R_1}^{R_2} n(r)\sigma_T dr = n_0\sigma_T r_s \ln(R_2/R_1). \quad (2)$$

In order to estimate the energy density of the scattered photon field, we should define first the luminosity of the accretion disc:

$$L_{\text{disc}} = \begin{cases} \epsilon \dot{m} \mathcal{M} L_{\text{Edd}} & \text{for } \dot{m} \gtrsim 0.1, \\ \epsilon \dot{m}^2 \mathcal{M} L_{\text{Edd}} & \text{for } \dot{m} \lesssim 0.1, \end{cases} \quad (3)$$

where  $L_{\text{Edd}} = 1.28 \times 10^{38} \text{ erg sec}^{-1}$  is the Eddington luminosity of one solar mass and  $\mathcal{M} = M_{\text{BH}}/M_{\odot}$ , where  $M_{\text{BH}}$  is the mass of the black hole and  $\epsilon$  is the efficiency of the conversion of the accreting mass into radiation. The case of  $\dot{m} \geq 0.1$  corresponds to a radiatively efficient disc and the case of  $\dot{m} < 0.1$  to a disc in an ADAF state.

Therefore, in the case where  $\tau_{\tau} \ll 1$  and  $R_1 \ll R_2$  the photon energy density of the scattered photons is

$$U_{\text{sc}} = \frac{L_{\text{disc}} \tau_{\tau}}{4\pi R_2^2 c}. \quad (4)$$

We will use this value as the external photon energy density when applying the one-zone leptonic model.

The other important quantity, i.e. the magnetic field strength, can be defined from the accretion power of the source, assuming that it is in some state of equipartition with the kinetic energy density of the accreted mass. Thus, if we define the accretion power of the source as

$$P_{\text{acc}} = \dot{m} \mathcal{M} L_{\text{Edd}}, \quad (5)$$

then the energy density of the magnetic field at the base of the outflow can be written as

$$U_{B_0} = \frac{\eta_b P_{\text{acc}}}{4\pi(3r_s)^2 c}, \quad (6)$$

where  $\eta_b$  is a proportionality constant ( $\eta_b < 1$ ) and assuming an inner disc radius of  $3r_s$ . Furthermore, in order to determine the strength of the magnetic field along the axis of the jet, we assume that

$$B = B_0(z_0/z), \quad (7)$$

where  $B_0$  is the value of the magnetic field at the base of the jet,  $z$  the distance from the central engine, and  $z_0 = 3r_s$ .

## 2.2 The radiation model

Having defined the external photon density and magnetic field, one can calculate the SED of the source in the case of a simple one-zone leptonic model. We assume, therefore, that the emission of the relativistic jet is dominated by a stationary single zone at some height  $z$  along the jet axis. The emitting region is assumed to be spherical with a radius  $R_b$  in its co-moving frame and it moves with a highly relativistic speed  $\beta c$ , giving it a Lorentz factor  $\Gamma = (1 - \beta^2)^{-1/2}$ . Its velocity makes an angle  $\phi$  to the line of sight, so the Doppler factor is  $\delta = [\Gamma(1 - \beta \cos \phi)]^{-1}$ .

Relativistic electrons are injected into the spherical volume and lose energy through synchrotron radiation on the embedded magnetic field of strength  $B(z)$  (given by equation 7) and IC scattering on internal and external photons.

Fig. 1 gives a schematical representation of the isotropization of the disc photons on the wind and their consequent upscattering to  $\gamma$ -rays by the relativistic electrons.

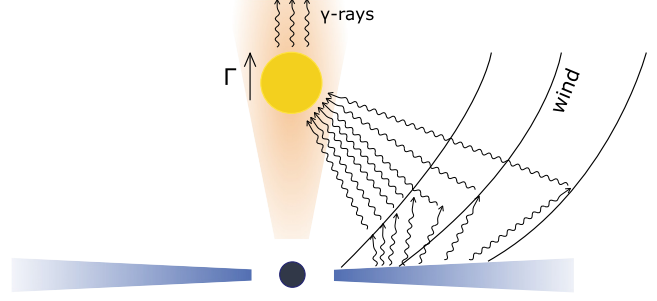


**Figure 1.** Schematic of the disc wind model for the  $\gamma$ -ray production (not in scale). Disc photons are scattered on wind particles and create an isotropic external photon field for the relativistic blob shown in yellow;  $\Gamma$  is the bulk Lorentz factor.

Furthermore, we assume that electrons are injected in the source with a broken power-law distribution given by

$$Q_e = \begin{cases} k_{e1} \gamma^{-s} & \text{for } \gamma_{\text{min}} \leq \gamma \leq \gamma_{\text{br}}, \\ k_{e2} \gamma^{-q} e^{-\gamma/\gamma_{\text{max}}} & \text{for } \gamma_{\text{br}} \leq \gamma \leq \gamma_{\text{max}}, \end{cases} \quad (8)$$

where  $L_{\text{inj}}^e = m_e c^2 \int_{\gamma_{\text{min}}}^{\gamma_{\text{max}}} Q_e(\gamma) \gamma d\gamma = \eta_e P_{\text{acc}}$ , where  $\eta_e$  is a proportionality constant. Here,  $\gamma_{\text{min}}$  and  $\gamma_{\text{max}}$  are the minimum and maximum electrons Lorentz factors, respectively,  $s$  and  $q$  the indices for the electrons' distribution before and after the break, respectively,  $\gamma_{\text{br}} = \frac{3m_e c^2}{4\sigma_{\tau} c t_{\text{dyn}} U_{\text{tot}}}$ , where  $t_{\text{dyn}} = \frac{R_b}{c}$  is the dynamic time-scale, while  $U_{\text{tot}}$  is the total energy density that is given by  $U_{\text{tot}} = U_B + U_{\text{ext}} + U_{\text{SSC}}$ , where  $U_B$  is the energy density of the magnetic field at position  $z$ ,  $U_{\text{ext}} = \Gamma^2 U_{\text{sc}}$  is the energy density of the scattered photons as measured in the co-moving frame and  $U_{\text{SSC}}$  is the energy density of the produced synchrotron photons, which is calculated self-consistently from the numerical code. In order to calculate the SED of scattered photons, we have assumed that the disc emits like a blackbody with a characteristic temperature  $T_{\text{disc}}$ . We also assume that  $\gamma_{\text{max}} \gg \gamma_{\text{br}}$  and for concreteness we use  $\gamma_{\text{max}} = 10^4 \gamma_{\text{br}}$ .

## 3 RESULTS

In order to calculate the blazar SED, we solve the kinetic equations of electrons and photons as described by Mastichiadis & Kirk (1995). As we pointed in the previous section, all input parameters required for the calculation of the spectrum are scaled with  $\dot{m}$  and  $\mathcal{M}$ . Thus, using equations (4), (7), and (8), one can write  $U_B \propto \frac{\dot{m}}{\mathcal{M}}$ ,  $U_{\text{ext}} \propto U_{\text{sc}} \propto \frac{\dot{m}^{\alpha+1}}{\mathcal{M}}$  ( $\alpha = 1$  for  $\dot{m} \geq 0.1$  and  $\alpha = 2$  for  $\dot{m} < 0.1$ ),  $\gamma_{\text{br}} \propto \dot{m}^{-1} (1 + \dot{m}^{\alpha})^{-1}$ , and  $L_e^{\text{inj}} \propto \dot{m} \mathcal{M}$ .

Furthermore, following Ghisellini et al. (2009), we relate the mass accretion rate to the blazar type. Thus, we assume that the case  $\dot{m} > 0.1$  corresponds to a radiatively efficient disc and therefore to an FSRQ object. On the other hand, the case  $\dot{m} \ll 0.1$  corresponds to a disc in an ADAF state and thus corresponds to a BL Lac object. Furthermore, BL Lac objects are divided in three subcategories, LBL, IBL, and HBL, which refer to a low, intermediate, and a high synchrotron peak frequency, respectively. We model these by using decreasing values of  $\dot{m}$ .

Table 1 shows the values of the calculated input parameters by varying only the mass accretion rate  $\dot{m}$ . In this example, we have kept the mass of the black hole constant. Fig. 2 depicts the obtained multiwavelength spectra and, as it can be seen, our simple, straightforward scalings reproduce the trend of the observed Blazar Sequence. Here, we have assumed constant values for  $\Gamma$  and  $\delta$  factors. For these cases, we use a constant temperature for the accretion

**Table 1.** Parameter values for different mass accretion rates in the case of  $\mathcal{M} = 10^9$ . All the values are in a logarithmic scale. The location of the source is at  $z = 1pc$ , we assume a spherical region for the external photon field between radii  $R_1 = 9 \times 10^{16}$  cm and  $R_2 = 3 \times 10^{19}$  cm. The efficiencies of the mass accretion rate to the magnetic field, electrons luminosity, and external photon field are  $\eta_b = 0.1$ ,  $\eta_e = 0.05$ , and  $\varepsilon = 0.5$ , respectively. The indices for the electron distribution are  $s = 2$  and  $q = 2.75$ . The bulk Lorentz factor is  $\Gamma = 30$  and the Doppler factor is  $\delta = 15$ . The characteristic temperature of the disc is  $T_{\text{disc}} = 3 \times 10^3$  K.

$\dot{m}$	$B(\text{G})$	$U_{\text{ext}} \left( \frac{\text{erg}}{\text{cm}^3} \right)$	$L_e^{\text{inj}} \left( \frac{\text{erg}}{\text{sec}} \right)$	$\gamma_{\text{br}}$	Blazar class
-0.5	-0.3	-1.4	45.2	2.3	FSRQ
-1.5	-0.8	-4.6	44.2	3.3	LBL
-2.5	-1.3	-7.6	43.2	6.5	HBL

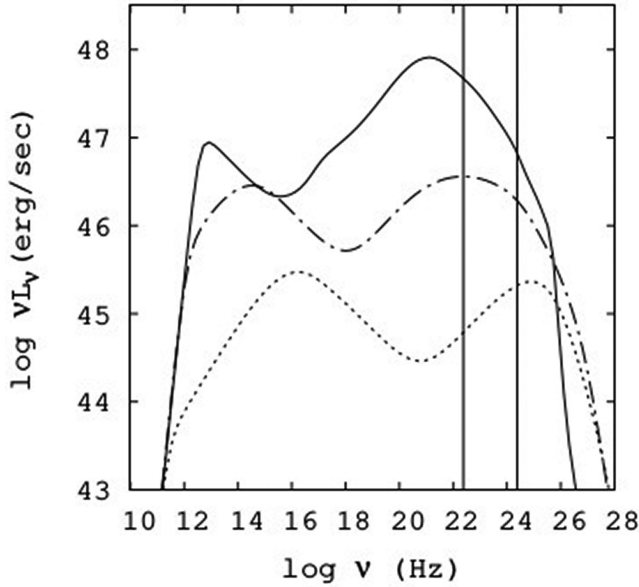


**Figure 2.** Multiwavelength spectra are calculated for different mass accretion rates. The straight, straight-dotted, dotted line refers to  $\log \dot{m} = -0.5$ ,  $\log \dot{m} = -1.5$ , and  $\log \dot{m} = -2.5$ , respectively. The black hole mass is  $\mathcal{M} = 10^9$  and the parameters' values are given in Table 1. The vertical lines show the Fermi energy band.

disc. In the case of high  $\dot{m}$ ,  $U_{\text{ext}}$  is also high and the source is Compton dominated and reproducing FSRQs objects. On the other hand, low values of  $\dot{m}$  correspond to low  $U_{\text{ext}}$  and as a result SSC scattering starts dominating over EC scattering. In this case, the SED of BL Lac objects is reproduced.

Furthermore, the observed peak of the synchrotron component for electrons with Lorentz factor  $\gamma_{\text{br}}$  will appear at  $\nu_{\text{pk}}^{\text{syn}} \propto \delta B \gamma_{\text{br}}^2$ . Using the relations described above, we find

$$\nu_{\text{pk}}^{\text{syn}} \propto \mathcal{M}^{-1/2} \dot{m}^{-3/2} / (1 + \dot{m}^\alpha)^2. \quad (9)$$

Therefore, while a low value of  $\dot{m}$  corresponds to lower values of  $B$ , the corresponding increase in  $\gamma_{\text{br}}$  leads to a higher value for  $\nu_{\text{pk}}^{\text{syn}}$ . On the other hand, as  $\dot{m}$  increases, despite the  $B$  increase, the decrease of  $\gamma_{\text{br}}$  shifts  $\nu_{\text{pk}}^{\text{syn}}$  to lower frequencies.

For a fixed observation band between  $\nu \sim 10^{22}$  and  $10^{24}$  Hz, as that of the *Fermi*-LAT, it is clear from Fig. 2 that the above scalings produce a progressive hardening of the  $\gamma$ -ray spectra by the progressive decrease of their index,  $\alpha_\gamma$ , with the decrease of the (normalized) accretion rate  $\dot{m}$ .

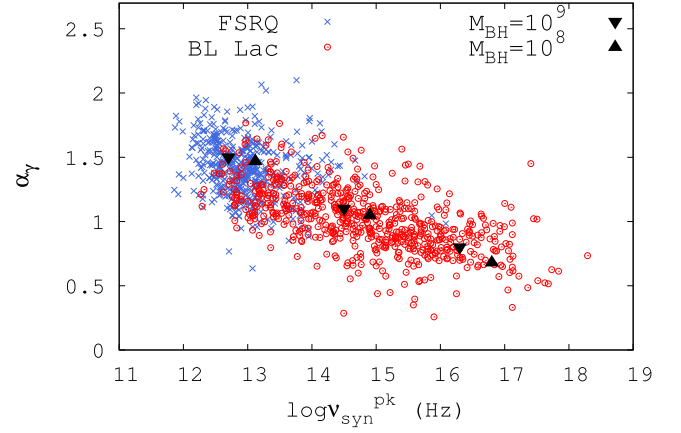


**Figure 3.** The variation of the  $\gamma$ -ray photon index  $\alpha_\gamma$  as a function of the frequency of the synchrotron peak  $\nu_{\text{syn}}^{\text{pk}}$  as shown in the 3LAC compilation. The triangular points show our model results for the two values of the  $M_{\text{BH}}$ . Three sets of points are produced for  $\log \dot{m}$  values of  $-0.5$ ,  $-1.5$ , and  $-2.5$  (left to right).

In Fig. 3, we superimpose the results of our model calculations on the compilation of  $\alpha_\gamma$  vs.  $\nu_{\text{pk}}^{\text{syn}}$  of 3LAC. We have chosen two values for the black hole mass,  $\mathcal{M} = 10^8$  and  $\mathcal{M} = 10^9$ , and three values of  $\log \dot{m}$ , namely  $-0.5$ ,  $-1.5$ , and  $-2.5$ . We have left all the other values associated with the emission, i.e.  $\Gamma$ ,  $\delta$ ,  $s$ ,  $q$ , constant. We see that, as argued qualitatively, the parameter that sets the range of variation of these two observables is the dimensionless accretion rate  $\dot{m}$ . The proximity of points differing in mass by a factor of 10 suggests that the mass is not the major driver of this relation (and the blazar main sequence generally).

#### 4 SUMMARY AND DISCUSSION

In this letter, we have shown that a one-zone leptonic model with a simple scaling of its input parameters on the (dimensionless) mass accretion rate,  $\dot{m}$ , can reproduce the basic trends of the Blazar Sequence, as first suggested by Fossati et al. (1998) and further elaborated by the *Fermi* 2LAC and 3LAC results. A key feature of our model is that the target photons necessary for the EC scattering are provided by the reprocessed disc radiation on an MHD wind. This is possible because the wind has a shallow density profile that results in a Thomson optical depth, which varies logarithmically with the outer disc radius but with normalization related directly to  $\dot{m}$ ; additionally, the strength of the magnetic field is also related to  $\dot{m}$ , thus reducing the freedom of the relevant parameters. Furthermore,  $\dot{m}$  determines also the efficiency of the disc luminosity, with a transition to an ADAF state for small values of  $\dot{m}$ . As a result, intrinsically powerful blazars, i.e. FSRQs, have larger ratios of external photon to magnetic field energy densities, and therefore are Compton dominated, while less intrinsically powerful ones, like BL Lacs that are assumed to be in an ADAF state, are synchrotron dominated. Fig. 2 shows how the multiwavelength spectra of these sources evolve with varying  $\dot{m}$  so that the corresponding  $\gamma$ -ray slope and  $\nu_{\text{pk}}^{\text{syn}}$  vary to cover a region consistent with that of the *Fermi* data (see Fig. 3).

The basic aim of this work was to reproduce the theoretical Blazar Sequence using a minimum number of free parameters. The fact that the strongest blazar correlation produced by the *Fermi* data compilation (see Fig. 3) involves only spectral attributes guided us to determine the most significant parameter. Note that, in order

to calculate the SED of the sources it is necessary to specify some physical quantities such as the magnetic field strength  $B$ , the characteristics of the electrons distribution ( $L_e^{\text{inj}}$ ,  $\gamma_{\text{min}}$ ,  $\gamma_{\text{br}}$ ,  $\gamma_{\text{max}}$ ,  $s$ ,  $q$ ), and the energy density of the external photon field  $U_{\text{ext}}$ . These physical quantities turn out to be functions of  $\dot{m}$  and the mass of the black hole,  $\mathcal{M}$ , (see Section 2). From our numerical calculations, we found that  $\dot{m}$  is the parameter that has the greatest contribution in the reproduction of Fig. 3, while the other parameter,  $\mathcal{M}$ , does not play a key role. We mention, however, that low values of  $\mathcal{M}$  can reproduce the multiwavelength spectra of FSRQs with low bolometric luminosity (Ghisellini et al. 2017). About the efficiencies  $\eta_b$ ,  $\eta_e$ ,  $\epsilon$  that also affect the physical quantities  $B$ ,  $L_e^{\text{inj}}$ ,  $U_{\text{ext}}$ , respectively, preliminary calculations have shown that their variations can reproduce the spread of the observables of Fig. 3 under the basic assumption of varying  $\dot{m}$ . Furthermore, we used ad hoc values of the slopes before and after  $\gamma_{\text{br}}$  so as to be in agreement with the  $\gamma$ -ray photon indices in Fig. 3. Finally, we found that varying the Doppler factor  $\delta$  has a similar effect as varying  $\mathcal{M}$  and for this reason we kept its value constant.

Despite the fact that the results of this work are similar to Finke (2013), the basic assumptions are different. In that paper the strength of the magnetic field is directly related to the energy density of the external photon field, while, in ours, quantities are related implicitly to  $\dot{m}$ .

To sum up, we have succeeded in reproducing the theoretical Blazar Sequence by varying only one free parameter ( $\dot{m}$ ) while keeping everything else fixed. We will examine systematically the effects of the secondary physical quantities in a future publication.

## ACKNOWLEDGEMENTS

DK acknowledges support by NASA ADAP and Fermi GI grants. We thank Dr. Maria Petropoulou for useful discussions and comments on the final manuscript. Also, we thank Dr. Stavros Dimitrakoudis for Fig. 1.

## REFERENCES

- Ackermann M. et al., 2011, *ApJ*, 743, 171  
 Ackermann M. et al., 2015, *ApJ*, 810, 14  
 Antonucci R. R. J., Miller J. S., 1985, *ApJ*, 297, 621  
 Behar E., 2009, *ApJ*, 703, 1346  
 Contopoulos J., Lovelace R. V. E., 1994, *ApJ*, 429, 139  
 Crenshaw D. M., Kraemer S. B., George I. M., 2003, *ARA&A*, 41, 117  
 Dermer C. D., Schlickeiser R., Mastichiadis A., 1992, *A&A*, 256, L27  
 Finke J. D., 2013, *ApJ*, 763, 134  
 Fossati G., Maraschi L., Celotti A., Comastri A., Ghisellini G., 1998, *MNRAS*, 299, 433  
 Fukumura K., Kazanas D., Contopoulos I., Behar E., 2010, *ApJ*, 715, 636  
 Fukumura K., Kazanas D., Shrader C., Behar E., Tombesi F., Contopoulos I., 2017, *Nature Astron.*, 1, 0062  
 Fukumura K., Kazanas D., Shrader C., Behar E., Tombesi F., Contopoulos I., 2018, *ApJ*, 853, 40  
 Ghisellini G., Celotti A., Fossati G., Maraschi L., Comastri A., 1998, *MNRAS*, 301, 451  
 Ghisellini G., Maraschi L., Tavecchio F., 2009, *MNRAS*, 396, L105  
 Ghisellini G., Tavecchio F., Foschini L., Ghirlanda G., 2011, *MNRAS*, 414, 2674  
 Ghisellini G., Righi C., Costamante L., Tavecchio F., 2017, *MNRAS*, 469, 255  
 Konigl A., Kartje J. F., 1994, *ApJ*, 434, 446  
 Marscher A. P. et al., 2010, *ApJ*, 710, L126  
 Mastichiadis A., Kirk J. G., 1995, *A&A*, 295, 613  
 Narayan R., Yi I., 1995, *ApJ*, 444, 231  
 Nieppola E., Valtaoja E., Tornikoski M., Hovatta T., Kotiranta M., 2008, *A&A*, 488, 867  
 Sbarrato T., Ghisellini G., Maraschi L., Colpi M., 2012, *MNRAS*, 421, 1764  
 Sikora M., Begelman M. C., Rees M. J., 1994, *ApJ*, 421, 153

This paper has been typeset from a  $\text{\TeX}/\text{\LaTeX}$  file prepared by the author.